Electrochimica Acta 507 (2024) 145170

Contents lists available at ScienceDirect

Electrochimica Acta

journal homepage: www.journals.elsevier.com/electrochimica-acta

Impact of functionalized titanium oxide on anion exchange membranes derived from chemically modified PET bottles

Varun Donnakatte Neelalochana [a], Eleonora Tomasino [a], Marcelo Augusto Malagutti [a], Ines Mancini [b], Andrea Chiappini [c], Sandeep Shadakshari [d], Maxwell W. Terban [e], Bernd Hinrichsen [e], Paolo Scardi [a], Narges Ataollahi [a,*]

[a] Department of Civil, Environmental, and Mechanical Engineering, University of Trento, Trento 38123, Italy
[b] Laboratory of Bioorganic Chemistry, Department of Physics, University of Trento, Via Sommarive 14, Povo, Trento 38123, Italy
[c] IFN-CNR CSMFO Lab and FBK Photonics Unit, Via alla cascata 56/c, Trento 38123, Italy
[d] Department of Chemistry, SJCE, JSS Science and Technology University, Mysuru, Karnataka 570 006, India
[e] Analytical and Material Science, BASF SE, Ludwigshafen D-67056, Germany

ARTICLE INFO

Keywords:
Anion exchange membrane
PET bottle
Functionalized TiO_2
Composite membrane
Electrochemical application
Alkaline stability
Circular economy

ABSTRACT

The accessibility of newly affordable materials has drawn significant attention to the anion exchange membrane (AEM) technology. However, developing a high-performance AEM with excellent hydroxide conductivity and long-term durability is still challenging. The present work aims to improve the overall properties of AEMs synthesized by chemical modification of Polyethylene terephthalate (PET) bottles as the starting material. The modified PET structure was confirmed using IR, NMR, and HPLC-ESIMS analyses. AEMs were developed by incorporating quaternary ammonium (QA) functional groups into the modified PET structure, necessary for transporting anionic species (OH^-). In addition, TiO_2 nanoparticles grafted with silane coupling agents containing amine functional groups were synthesized via the sol-gel method and embedded in the polymer matrix. Then, the prepared nanocomposite membranes were thoroughly characterized, and the results displayed an overall improvement in the membrane's physicochemical properties. The composite membrane with 3wt% content of nanoparticle ($NC_{3\ \%}$/M-PETm) showed remarkable conductivity, reaching 126 mS/cm at 80 °C, doubling the value of pristine membranes (64 mS/cm) while also displaying alkaline stability, retaining up to 92.2 % of conductivity after 20 days in harsh 2 M KOH at 80 °C. These results proved the suitability of these membranes for electrochemical energy applications. This innovative approach offers potential cost savings in preparing the new membranes while aligning with sustainable and circular economy principles.

1. Introduction

Anion exchange membranes (AEMs) have received much attention in the last few years, particularly in the field of energy storage and conversion. Some of the main electrochemical applications include water electrolyzers, fuel cells, water desalination, and redox flow batteries [1–6]. Despite the advantageous production costs compared to proton exchange membranes (PEMs), AEMs notably suffer from poor chemical stability when operated at high pH levels and exhibit lower ionic conductivity [7–10]. The design of robust, stable, and highly conductive membranes is the key point for developing efficient AEMs, able to compete with PEMs in the electrochemistry application [11].

Diverse polymer structures have been proposed for the preparation of AEMs, encompassing polyphenylene oxide PPO (Fumatech FAA series) [12], poly (4-vinylbenzyl chloride-co-styrene) (Sustainion® X37–50) [13], methylated polybenzimidazoles PBI (Aemion® series) [14] and many others. Recently, a lot of efforts has been devoted to developing innovative materials that might emerge because of the outstanding properties, the competitive price, or the sustainable production process. For this purpose, the chemical modification of plastic wastes might be a valid solution. Chemical recycling of PET stands out as an innovative and efficient method for the requalification of plastic waste [15], allowing the production of new materials with tunable features. The aminolysis process deals mainly with a nucleophilic attack by primary amines on ester bonds of PET, leading to a scission of the polymer backbone [16]. Introducing amine and amide groups to the

* Corresponding author.
E-mail address: narges.ataollahi@unitn.it (N. Ataollahi).

https://doi.org/10.1016/j.electacta.2024.145170
Received 1 August 2024; Received in revised form 5 September 2024; Accepted 28 September 2024
Available online 29 September 2024
0013-4686/© 2024 The Author(s). Published by Elsevier Ltd. This is an open access article under the CC BY license (http://creativecommons.org/licenses/by/4.0/).

original PET structure imparts some desirable properties, such as improved wettability and thermal stability [17]. Moreover, the presence of additional functional groups on the previously inert material provides active sites for further reactions and possible ionic interactions, paving the way for the synthesis of AEMs constituent polymers. Aminolysis reactions have been extensively discussed in the literature, and different valuable materials have been synthesized for a variety of uses, including fabric fibers [17], biomedical [18], and many other industrial applications [19,20]. Nevertheless, very little research has been conducted on the use of recycled PET for electrochemical applications [21]. In our previous work, we proved the potential of chemically modified PET for producing AEMs [22]. However, the obtained AEM shows moderate conductivity and potential for improved stability.

Several approaches have been proposed to improve membrane properties and long-term durability. Some of these strategies include crosslinking, polymer blending, and the addition of nanoparticles [23,24]. Incorporating nanoparticles (NPs) into the membrane matrix is a well-established technique to improve essential properties, enjoying both the advantages of inorganic and organic moieties [25,26]. The use of various inorganic NPs, such as titanium dioxide (TiO_2), zirconium dioxide (ZrO_2), and silicon dioxide (SiO_2), has been extensively discussed in the literature [27–30]. While these NPs contribute to a discernible enhancement in thermal and mechanical stability, an overall decline in ionic conductivity is generally observed at higher loadings. This decline is attributed to the nanoparticle's tendency to agglomerate within the host matrix, blocking the pathway for ion mobility [31]. Grafting inorganic nanoparticle surfaces with organic functional groups is a promising approach to overcome these limitations and tailor the resulting material's properties. The essential features of the original inorganic particle, including dimensional, thermal, and mechanical stability, are retained after surface modification [32–34]. At the same time, introducing functional groups compatible with the polymer chains enhances the dispersion of the filler, allowing for greater uniformity of the membrane. Moreover, additional charged groups could increase the membrane's ion exchange capacity (IEC) and water retention during operating conditions, leading to higher conductivity [35,36].

Only some reports on composite AEMs containing functionalized nanoparticles can be found in the literature. Lee et al. [37] synthesized composite membranes using quaternized poly (arylene ether ketone) containing functionalized TiO_2 NPs. The addition of modified NPs resulted in a well-defined phase separation of the membrane, which enhanced the ionic conductivity when the content of NPs was no >5 wt %. In addition, thermal and mechanical properties displayed a significant improvement. Ataollahi et al. [33,38] demonstrated a notable improvement in the performance of polyamine-based AEMs after the addition of SiO_2 nanoparticles grafted with (3-aminopropyl)triethoxysilane (APTES). The nanoparticles induced a reinforcement effect and increased thermal stability and ionic conductivity. Simari et al. [39] prepared nanocomposite membranes consisting of quaternized polysulfone (qPSU) and silica-based Nanoscale Ionic Materials (NIMs). The silica surface grafted with the functional groups enables the tuning of physicochemical properties of nanoparticles, which eventually induced significant improvement of the AEMs. The most relevant result was the improvement of >50 % ionic conductivity after NIMs addition. Furthermore, a substantial enhancement of mechanical and alkaline stability was discerned.

In the current work, we aim to enhance the physicochemical properties of PET-based anion exchange membranes by incorporating variable percentages of functionalized titanium oxide nanoparticles (F-TiO_2). The pristine membranes have been prepared by chemically modifying the PET bottles through a one-pot reaction. The composite PET-AEMs were prepared by incorporating functionalized nanoparticles (F-TiO_2). To allow a homogeneous distribution of fillers and to provide more NH_2-sites for anions transport, TiO_2 nanoparticles have been functionalized via a sol-gel approach, grafting (N1-(3-trimethoxysilylpropyl) diethylenetriamine) (3-silane) [40,41]. The long alkyl chains introduced by this reagent are expected to induce greater microphase segregation, ion conductivity, and alkaline stability [39,42]. TiO_2 has been selected as an inorganic material because of its availability, low cost, chemical stability, hygroscopic ability, and non-toxicity [43,44]. Moreover, it can be easily modified with organic functional groups, and, among other metal oxide nanoparticles, it presents a large specific surface area responsible for water adsorption and grafting sites [45].

This study conducted a detailed characterization of functionalized nanoparticles and assessed their compatibility with the PET-based membrane. Subsequently, the physicochemical and microstructural properties of these membranes were investigated. The results displayed an overall improvement in the anion exchange membrane's properties. In particular, the composite AEM displayed significantly enhanced OH^- conductivity compared to the pristine one.

2. Experimental section

2.1. Chemicals and materials

PET was sourced from discarded water bottles. Chemicals including 1,2-diaminopropane (99 %), 1,1,3,3,3-hexafluoroisopropanol (99 %), *N,N*-dimethylacetamide (99 %), iodomethane (99 %), ammonium hydroxide solution (30 %), potassium hydroxide (90 %), sodium nitrate (99 %), 1-methyl-2-pyrrolidinone (99 %), dimethyl sulfoxide (99.9 %), *N,N*-dimethyl formamide (99 %), silver nitrate (99 %), potassium chromate (99 %), N1-(3-trimethoxysilylpropyl) diethylenetriamine (97 %), Anatase Titanium(IV) oxide (99.7 %), and potassium chloride (99 %), were bought from Sigma-Aldrich. Sodium hydroxide (98.8 %), hydrochloric acid (37 %), acetone (99.5 %), and ethanol (99.8 %) were acquired from Honeywell. Propanol (99.9 %) was purchased from Carlo Erba reagents. Methanol was obtained from the Chem Lab NV, and throughout the experiment ultra-pure (u.p.) water was utilized.

2.2. Conversion of PET to aminolysis products (M-PET)

The chemical modification of PET polymer was conducted via a one-pot aminolysis reaction. PET bottles were cut into small fragments, washed with distilled water and ethanol, and dried at 40 °C for 2 h. Then, 5 g of PET flakes were treated with 15 mL of 1,2-diaminopropane (DAP) to reach a PET/DAP molar ratio of 1: 6.76 in a flask connected to a reflux condenser. The reaction was maintained at 140 °C for 4 h, and no catalysts or solvents were employed. To further extend the reaction, 5 mL of methanol was introduced into the solution at 40 °C and stirred at refluxing conditions for 3 more hours. After reaching room temperature, the mixture yielded a viscous, yellowish-green liquid. Subsequently, it was filtrated, and the excess DAP was removed through high vacuum drying over 24 h. Finally, the viscous solution underwent further drying at 65 °C and it was grinded to obtain a yellowish powder. The obtained product from depolymerization of PET polymer will be referred to as modified PET (M-PET). The schematic monomeric and oligomeric products are reported in Scheme 1.

2.3. Synthesis of functionalized TiO_2

The grafting of silane functional groups onto the nanoparticle's surface was conducted via the sol-gel method. This method consists of a low-temperature procedure that allows for coating nanoparticles' surfaces cost-effectively, easily, and in a controlled manner [46]. TiO_2 NPs were dried at 80 °C to remove possible adsorbed moisture. Following this, 1 g of TiO_2 was suspended in 30 mL of propanol, and then 50 mL of NH_4OH aqueous solution was dropped into the reaction mixture to attain a pH value of 10 and stirred for 2 h at room temperature. Afterward, 15 mL of N1-(3-trimethoxysilylpropyl) diethylenetriamine (3-silane) was added, and stirring continued overnight. The obtained solution was left to rest for one day to allow gelation. The gel was then

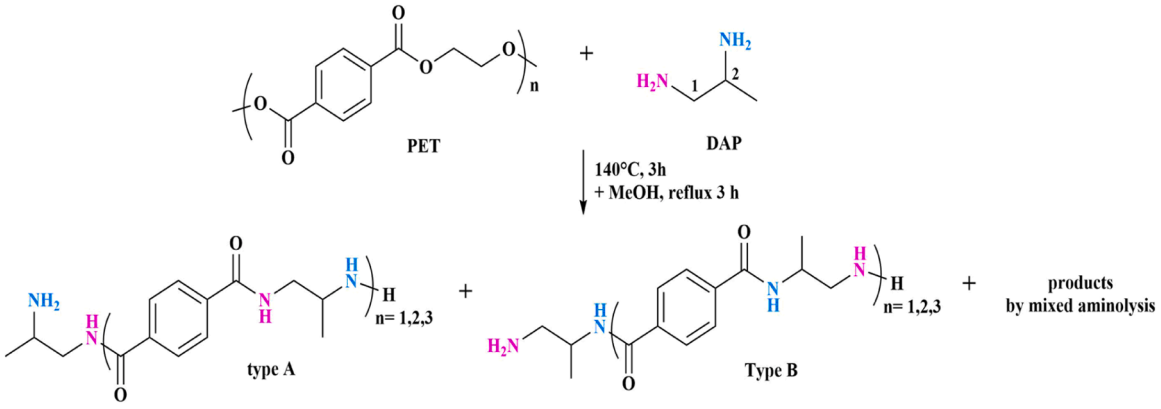

Scheme 1. Schematic representation of PET reaction with 1,2-diaminopropane (DAP) producing M-PET as monomers and oligomeric products.

centrifuged using the MPW-380 centrifuge at 8000 rpm for 20 min. The solid part was separated and subsequently washed with ethanol to remove the excess 3-silane by centrifuging at 6000 rpm for 10 min. The final material (F-TiO_2) was obtained as a powder after drying at 80 °C for 5 h. A schematic view of the synthesis procedure and the reaction mechanism is displayed in Fig. 1.

2.4. Preparation of nanocomposite membranes

Nanocomposite membranes (NC/M-PETm) were prepared by embedding F-TiO_2 nanoparticles into the M-PET matrix using a solution casting technique. Variable contents (0.5, 1, 2, 3, and 4 %) of F-TiO_2 and 0.3 g of M-PET were mixed and finely ground altogether. No >4wt% of nanoparticles were used since at this content we observed a reduction in IEC (1.58 $mmolg^{-1}$) and conductivity (53 mS/cm at 20 °C). Additionally, an excess of filler may hinder the transport of anionic species by blocking the water channels and making the functional groups inaccessible [25]. Next, 2 mL of HFIP solvent was added, and the solution was kept first in a sonication bath (Bandelin Sonorex) for 30 min and then stirred for 3 h at 40 °C. The final solution was poured into a square glass mold, letting the solvent evaporate for 24 h to form the membrane. Subsequently, the dry membranes were methylated by soaking them in iodomethane for 24 h (NC/M-PETm$_{\bar{I}}$) and excess CH_3I was washed away with water. The methylated membranes underwent immersion in a 1 M KOH solution for 24 h in an N_2 environment, converting the membranes into OH^- form (NC/M-PETm$_{\bar{I}OH}$). Different solvents were used for the solubility test during membrane preparation, as shown in Supplementary Information (S1) **Table S1**. Among them, HFIP was selected, as it enabled the formation of membranes with enhanced flexibility and better morphology [47,48]. The physical morphologies of the membranes with and without nanoparticles are shown in **Figure S1**.

The comprehensive details regarding the instrumentation and procedures are elaborated in the Supplementary Information (S2).

3. Results and discussion

3.1. Electrospray ionization mass spectrometry (ESI-MS) and HPLC-ESIMS analyses

The depolymerization of PET by aminolysis is based on the nucleophilic substitution of the amino group on the ester group of the polymer. The DAP reagent has two primary amino groups and products with a or b-type structures (Scheme 1) are expected for the monomer, with ratios that depend on the partial selectivity due to the lower steric hindrance of the amino group on the C-1 carbon of the DAP. Furthermore, the formation of oligomers is possible, with *a, b*, or mixed-type structures.

ESIMS spectrum of the modified PET samples (M-PET) recorded in negative ion mode showed the signals at *m/z* 277 ascribable to the $[M-H]^-$ ion for the monomer and a less intense signal at *m/z* 481 corresponding to $[M-H]^-$ ion with *M*= molecular mass of the dimer (**Figure S2**). More detailed results were obtained by HPLC-ESIMS analysis. The UV chromatogram displayed an intense peak at retention time t_R =3.0 min and minor peaks in the range of 7–10 min (Fig. 2a). The extracted ion chromatograms indicated the signal at t_R =3.0 min associated with *m/z* 276.8 corresponding to the monomer (Fig. 2b), three signals around t_R =7 min all associated to *m/z* 481.4 corresponding to three dimers with different structures (Fig. 2c), and two signals around t_R =10 min associated to the same *m/z* 685.8 corresponding to two different trimers (Fig. 2d), In summary this analysis allowed to detect the complexity of aminolysis products as components of M-PET. Although the relative abundance cannot be evaluated rigorously due to the different ionization properties of monomer, dimers, and trimers, the

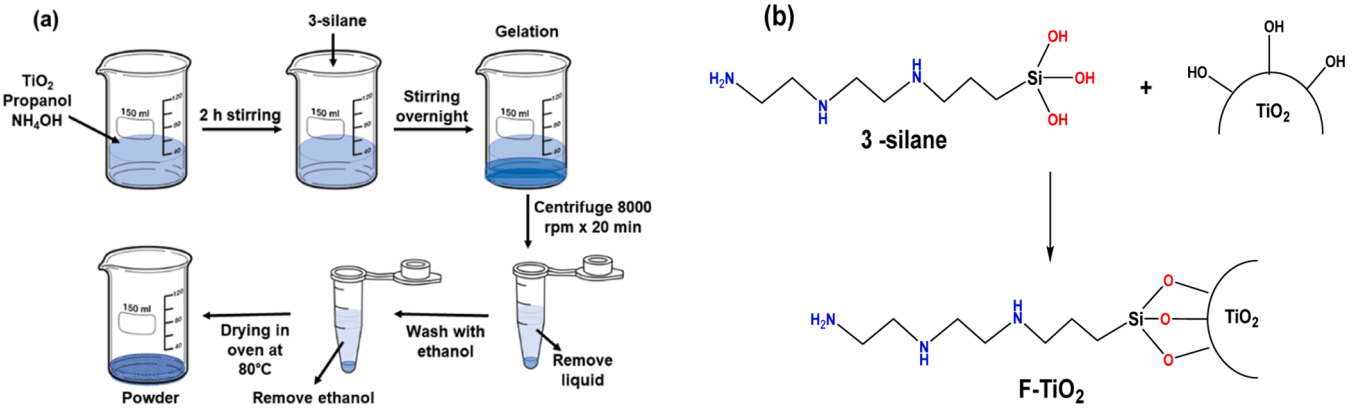

Fig. 1. (a) Scheme illustrating the synthesis process of F-TiO_2 via the sol-gel method. (b) The reaction mechanism of synthesis F-TiO_2.

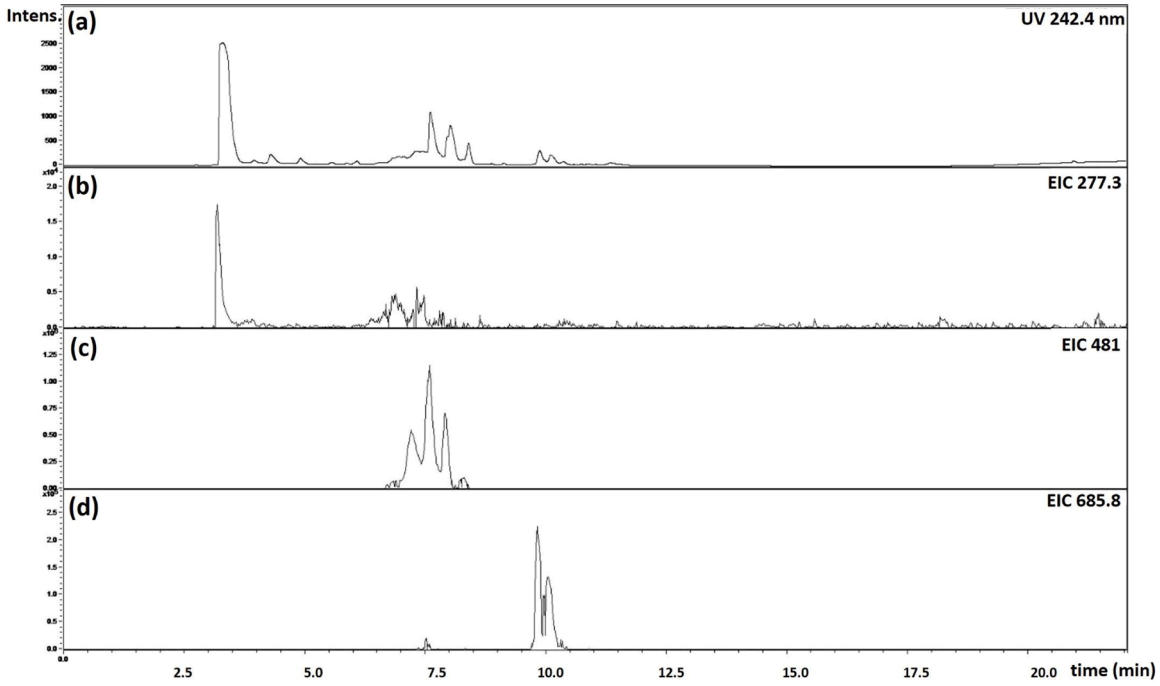

Fig. 2. Online HPLC-ESI (-) MS analysis of M-PET: (a) chromatographic profile at 242 nm and extracted ion chromatograms (EIC) at (b) *m/z* 276.8, (c) *m/z* 481.4 and (d) *m/z* 685.8.

data show the presence of one main monomer ($C_{14}H_{22}N_4O_2$, MM = 278.3), followed by three minor dimers ($C_{25}H_{34}N_6O_4$, MM = 482.5) and two much smaller trimers ($C_{36}H_{46}N_8O_6$, MM =686.8).

3.2. NMR analysis

The ^{1}H NMR spectrum of aminolysis products confirmed the presence of different similar structures as shown in Fig. 3a, already detected specifically in HPLC-ESIMS analysis. The signals in the regions 7.95–7.80 ppm are ascribed to aromatic protons. Due to the symmetric structure of monomers of type *a* and *b* and of the expected main oligomers, each of the most intense signals at 7.91, 7.87 and 7.83 ppm must be a singlet for each compound. The product mixture is also confirmed by the signals in the region 1.20–0.95 ppm corresponding to the data for the methyl groups, all detected as doublets with $J = 6.2$ Hz. The most intense is the doublet at 0.98 ppm, present about in 55:45 ratio with the doublet at 1.15 ppm, attributable to the methyl groups in the monomer of type *a* and *b* (Scheme 1), respectively as supported also by the simulated spectra by ChemDraw Ultra 12.0 software. If MS analysis cannot distinguish among these kinds of isomers with the same molecular mass, NMR spectroscopy can provide more details for assigning their structures. Additionally, there are two minor doublets at 1.18 and 1.11 ppm, attributable to the internal methyl group of the dimers and trimers. The approximately 1:1.5 ratio between aromatic and methyl signals available from their integrals is in line with the corresponding four aromatic and six methyl protons for the most abundant monomers. The multiplets in the region 4.5–3.0 ppm are due to the protons of the amino chains.

The ^{13}C NMR spectrum (Fig. 3b) showed signals at 165.80 and 161.6 ppm corresponding to the carbonyl of two different amides, attributable to the main monomers (Scheme 1), signals for the aromatic carbon atoms in the region 138–123 ppm, the signals at 48.0 and 46.3 to the CH and CH_2 amino chains and the signals at 21.9, 21.3 and 17.9 to different kind of methyl groups. Further support for the assignments came from bidimensional hetero-correlations experiments. In particular, the HSQC (Heteronuclear Single Quantum Coherence) spectrum indicated the directly linked $^{1}H/^{13}C$ nuclei for the methyl groups 0.98/ 21.3, 1.11/ 17.9, and 1.18/ 21.9 ppm. Significant $^{1}H,^{13}C$ long-range correlations detected by HMBC (Heteronuclear Multiple Bond Correlation) experiment are methyl protons at 0.98 ppm with 46.3 ppm, aromatic protons at 7.91 and 7.87 ppm with the C=O at 165.80 and 161.6 ppm, respectively (**Figure S3).**

3.3. FTIR analysis

FTIR analyses carried out on PET flakes and M-PET powder further support the effectiveness of the aminolysis reaction. The spectra and detailed descriptions for PET, M-PET, M-PETm and M-PETm(I^-) are reported in the SI (**S3, Figure S4 & S5**), and the band assignments using the correlative method are reported in **Table S2**.

Fig. 4 and **Table S3** show the effective functionalization of TiO_2 nanoparticles, supported by i) the new peaks in the F-TiO_2, typically observed in the spectrum of the 3-silane coupling agent, that suggest a successful surface functionalization of TiO_2; ii) the peaks around 3280 cm^{-1} characteristic of the N—H stretching in primary and secondary amines; iii) the peaks at 2940–2840 cm^{-1} attributable to C—H stretching in the alkyl chain. Additionally, various signals of medium and weak intensities in the region between 1180 and 1575 cm^{-1} correspond to C—H bending, NH_2 scissoring, N—H stretching/bending, and C—N stretching [49]. The sharp peak at 1077 cm^{-1} in 3-silane and 1121 cm^{-1} in F-TiO_2 is typical of the C—N stretching in primary amine. The broad signal below 800 cm^{-1} is due to Ti-O-Ti bonds and is present in pristine and modified nanoparticles [31,50]. Moreover, the appearance of the new signal at 1020 cm^{-1} in modified NPs is assigned to Ti-O-Si bond stretching [50], which confirms the coupling reaction of 3-silane occurring at the surface of the oxide. Additionally, the surface functionalization of TiO_2 was also demonestarted by the UV–Vis analysis as illustrated in detail in the SI, in **Section S4, Figure S6**. The spectrum of nanocomposite (NC_3 %/M-PETm) is displayed in green in Fig. 4. The membrane shows a broad peak around 3500–3200 cm^{-1}, overlapping with the N—H peaks, which is ascribed to the presence of some water molecules absorbed in the sample. The strong peaks detected in NC_3 %/M-PETm spectrum at 1200–1100 cm^{-1}, overlapping with those of 3-silane, are due to C—N vibrations of the silane coupling agents. and

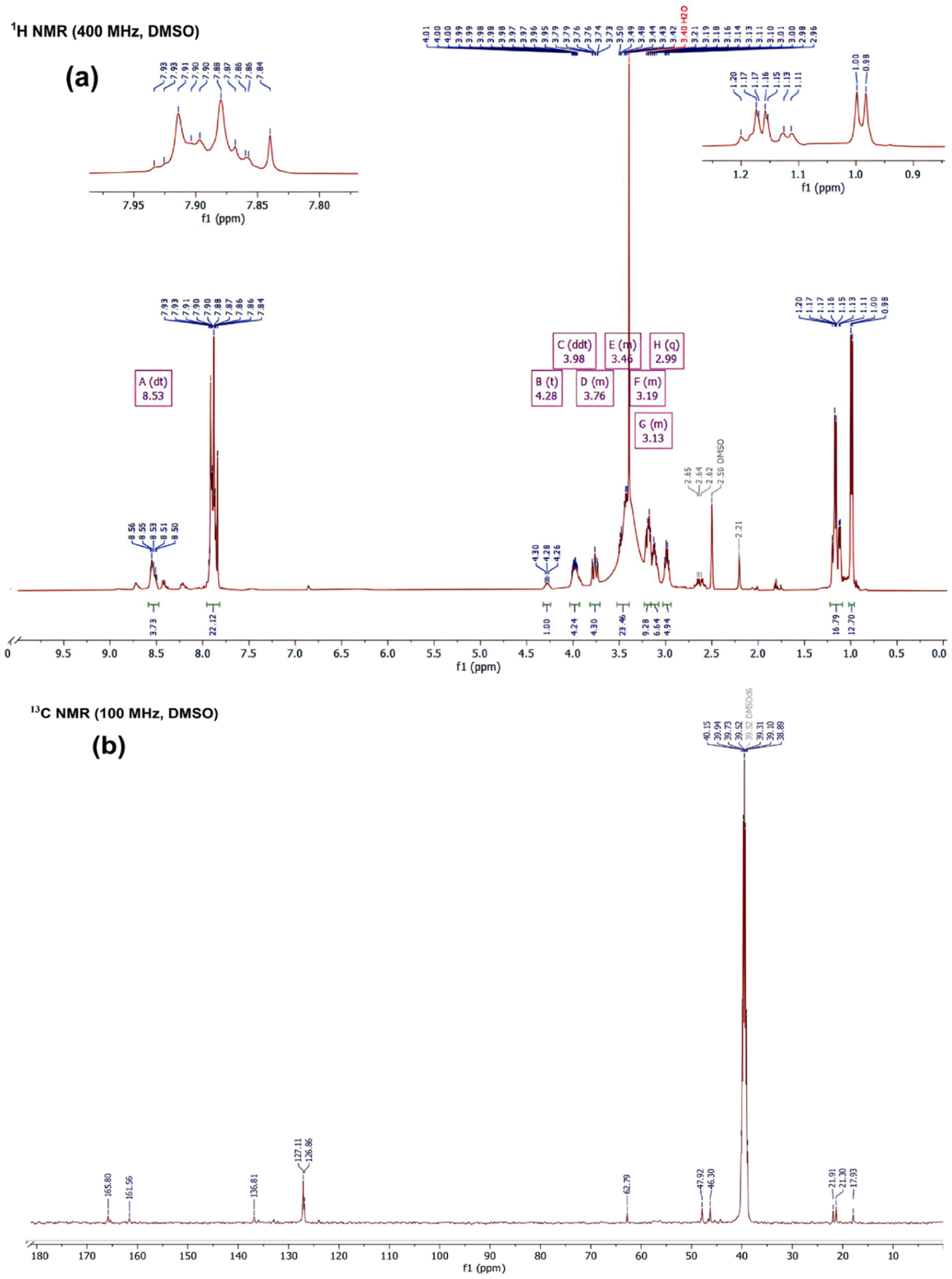

Fig. 3. (a) ^{1}HNMR (400 MHz) and (b) ^{13}C NMR (100 MHz), spectra for the modified PET in DMSO-d_6.

the signal below 800 cm^{-1}, may indicate the interaction of modified TiO_2 with the polymer host.

3.4. XRD analysis

The laboratory XRD diffraction pattern was employed to estimate the quantity of amorphous components, including functional groups on the TiO_2 surface. Fig. 5 shows the XRD pattern of F-TiO_2 (70 wt%), mixed with the spike phase of ZnO (30 wt%). The goodness of fit (GoF) reached 1.18, in good agreement with the structural models of anatase TiO_2 (*I41/amd,* PDF #01–086–1157) and zincite ZnO (*P63mc*, PDF# 04–003–2106). Secondary peaks of Brookite TiO_2 (*Pbca*, PDF# 04–007–0758) are observed in the pattern, corresponding to <3wt%, within the limit of XRD detection. A subtle feature in the background

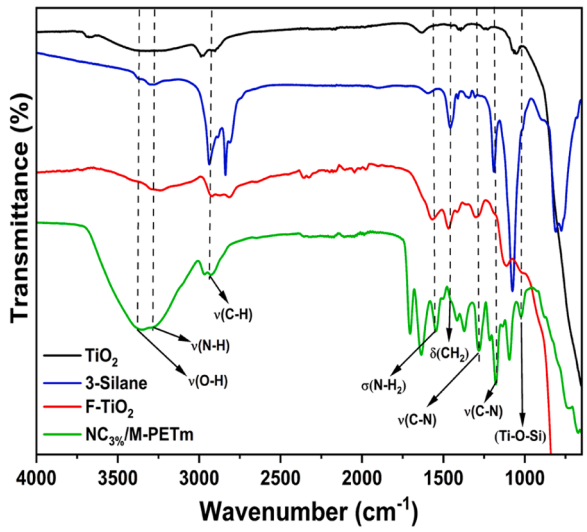

Fig. 4. FTIR spectra of pristine TiO_2,3-silane, F-TiO_2, and $NC_{3\ \%}$/M-PETm.

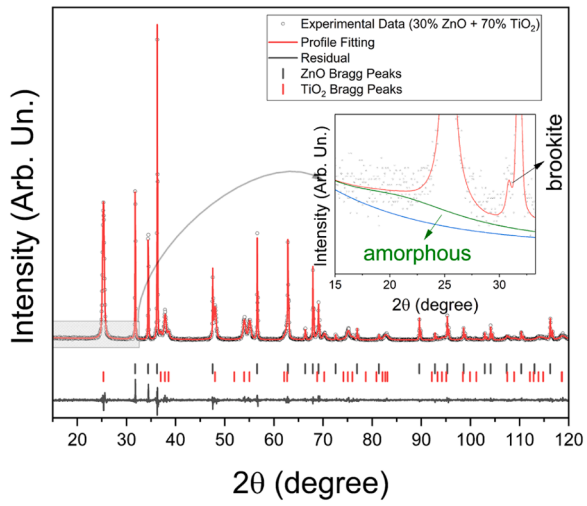

Fig. 5. XRD pattern for the F-TiO_2 (70 %) + ZnO (30 %) obtained using CuKα radiation. Dots represent the experimental data, red lines the Rietveld profiled fitting, and black lines the residuals. The markers represent the Bragg peaks of ZnO (black) and TiO_2 (red). Inset: zoomed area of the grey rectangle. In blue is the background profile, adjusted using the pure TiO_2, and green is the amorphous contribution from the functional group. The Brookite Bragg peak is indicated in the figure.

indicates the presence of an amorphous phase (Fig. 5 inset), attributed to the surface functionalization of TiO_2 with the silane groups, among other organic contributions [51]. The amorphous content reached 18 (±2)% in weight according to the internal standard method employed in TOPAS [52].

The XRD patterns obtained from the high-resolution synchrotron measurements provide a better visualization of the amorphous component in the pattern due to its higher beam brilliance. The amorphous contribution, separated from the diffuse component [53] and background, is available in **Figure S7**. By comparing the pristine TiO_2 and F-TiO_2 patterns, a broad signal is spotted near the base of the main TiO_2 peak, which is attributed to the functional groups (**Figure S8**). Whole powder pattern modelling (WPPM) [54] of the high-resolution synchrotron data attains the effect on structural and microstructural properties before and after modification. The functionalization does not affect the c/a ratio of the TiO_2 lattice parameters, presenting values of 2.51044±2 and 2.50951±2 before and after grafting, respectively. Lattice parameters are tabulated in **Table S4**. Regarding the crystalline domain, an average crystallite size (standard deviation) of 19.2 ± 1 (6.44±8) nm and 18.5 ± 1(6.46±8) nm was observed for pure and modified TiO_2, respectively, modeled using the WPPM approach (vide **Figure S9**). This means that no significant microstructure deviation after the grafting occurred. Additional evidence on the apparent lack of modifications of the TiO_2 nanoparticles caused by functionalization can be obtained by the PDF analysis of the F-TiO_2 data, using the data collected at 0.3 m SDD. The PDF fitting is plotted in **Figure S10** of the SI, showing no extra features other than the TiO_2 crystalline contribution. With the 0.3 m SDD data, it is also possible to extract information on the local dynamical structure of TiO_2, represented in the form of Debye-Waller (DW) parameters in the Bragg component and thermal diffuse scattering model for the diffuse part [53]. Ti presented a DW parameter of 0.34(±2) $Å^2$ and O of 0.48(±6) $Å^2$, being similar before and after functionalization (parameters of fitting in **Table S5**).

Smaller particles are expected to enhance water retention and conductivity due to the larger specific surface area responsible for water adsorption and surface functionalization [55]. In addition, the size of the inorganic fillers significantly influences the membrane's properties, providing an improved polymer-nanoparticle interaction, which endorses a better dispersibility of fillers and enhances the morphology. Therefore, the XRD and PDF results confirm that no alteration in the microstructural properties of TiO_2 is identifiable after the functionalization and maintenance of its properties.

3.5. TEM and SEM analyses

TEM and SEM micrographs were taken to investigate the morphology of nanoparticles and membranes, respectively. Figs. 6 (a,b) demonstrate the tendency of TiO_2 and F-TiO_2 to agglomerate. The formers aggregate more and tend to form larger clusters than functionalized nanoparticles due to the stronger electrostatic interaction. These interactions are reduced after the grafting of 3-silane on the surface, and the appearance of single nanoparticles is shown in **Fig S11. Figs 6(c,d)** display individual clusters of nanoparticles. In both cases, the average particle size is around 20 nm. The halo surrounding the F-TiO_2 is a clue for organic compounds coating the surface [56].

Fig. 7 shows pristine and composite membranes' surface and cross-section SEM micrographs. Pristine membranes (a,c) demonstrate a smooth and compact structure without the evidence of defects and irregularities. Composite membranes (b,d) exhibit a homogeneous dispersion of nanoparticles. Even though some NPs clusters are present, due to their natural tendency to aggregate [35], small and isolated particles are still visible. Overall, the compact morphology of the polymer matrix and the lack of phase separation prove the compatibility of the two materials. The EDX mapping of the membrane (**Figure S12a**) and the elemental analysis of F-TiO_2 (**Figure S12b**) attest to the presence of N and Si of silane groups.

3.6. IEC, WU, SR, and hydration number

The assessment of IEC, WU, and SR is essential to evaluate the membrane properties. Fig. 8 and **Table S6** illustrate the measured values for M-PETm$_{\bar{I}OH}$ and NC/M-PETm$_{\bar{I}OH}$ with different contents of nanoparticles. Fig. 8a shows the obtained IEC values that are in the range of 1.36–1.62 mmol g^{-1}, exhibiting an upward trend with increasing F-TiO_2 content up to 3 wt% due to the increased number of cationic sites introduced with nanoparticles [57]. WU and SR are essential features affecting the morphology, conductivity, and mechanical stability of the AEMs [31]. The formation of developed and interconnected water channels is desired since water molecules serve as vehicles for ion transport and provide sites for ion hopping through hydrogen-bond networks. However, excess water absorption can compromise mechanical strength and stability, and unrestrained membrane swelling should be avoided. **Table S5** and **Figure 8(b-d)** report temperature-dependent

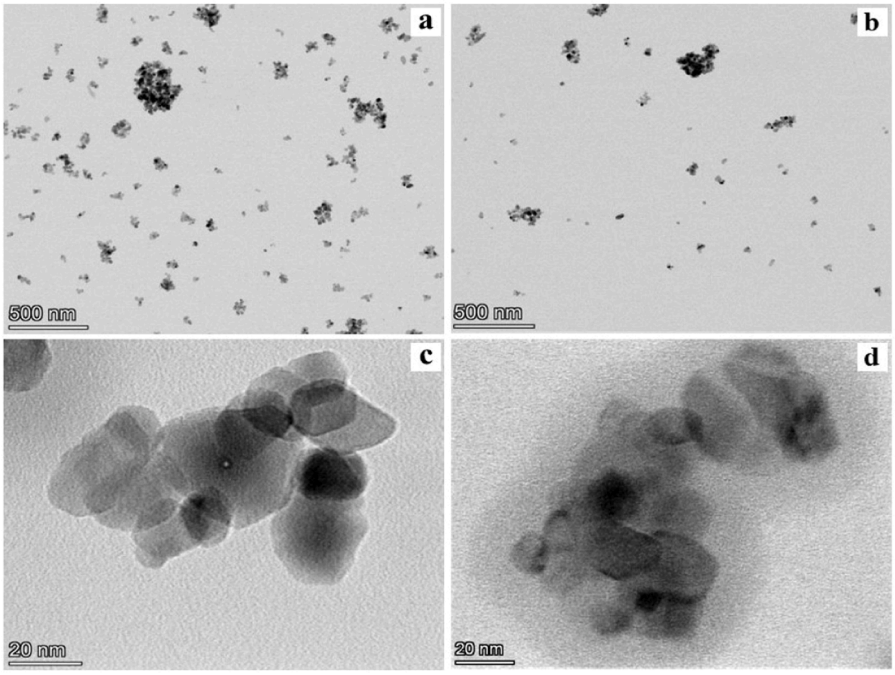

Fig. 6. TEM images of (a,c) TiO_2 and (b,d) F-TiO_2.

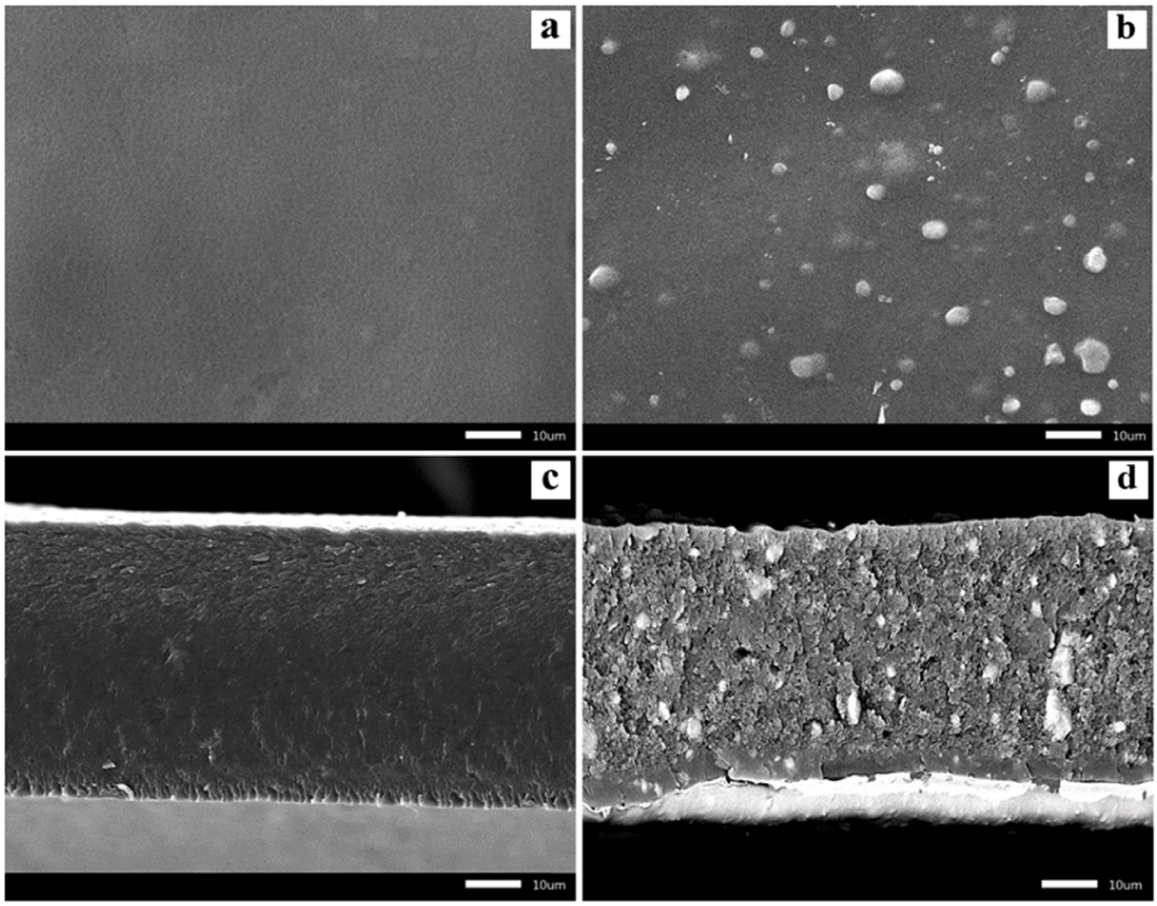

Fig. 7. SEM micrographs of the surface and cross-section of pristine M-PETm (a,c) and composite $NC_{3\ \%}$/M-PETm (b,d) membranes, at magnification of 1000 times.

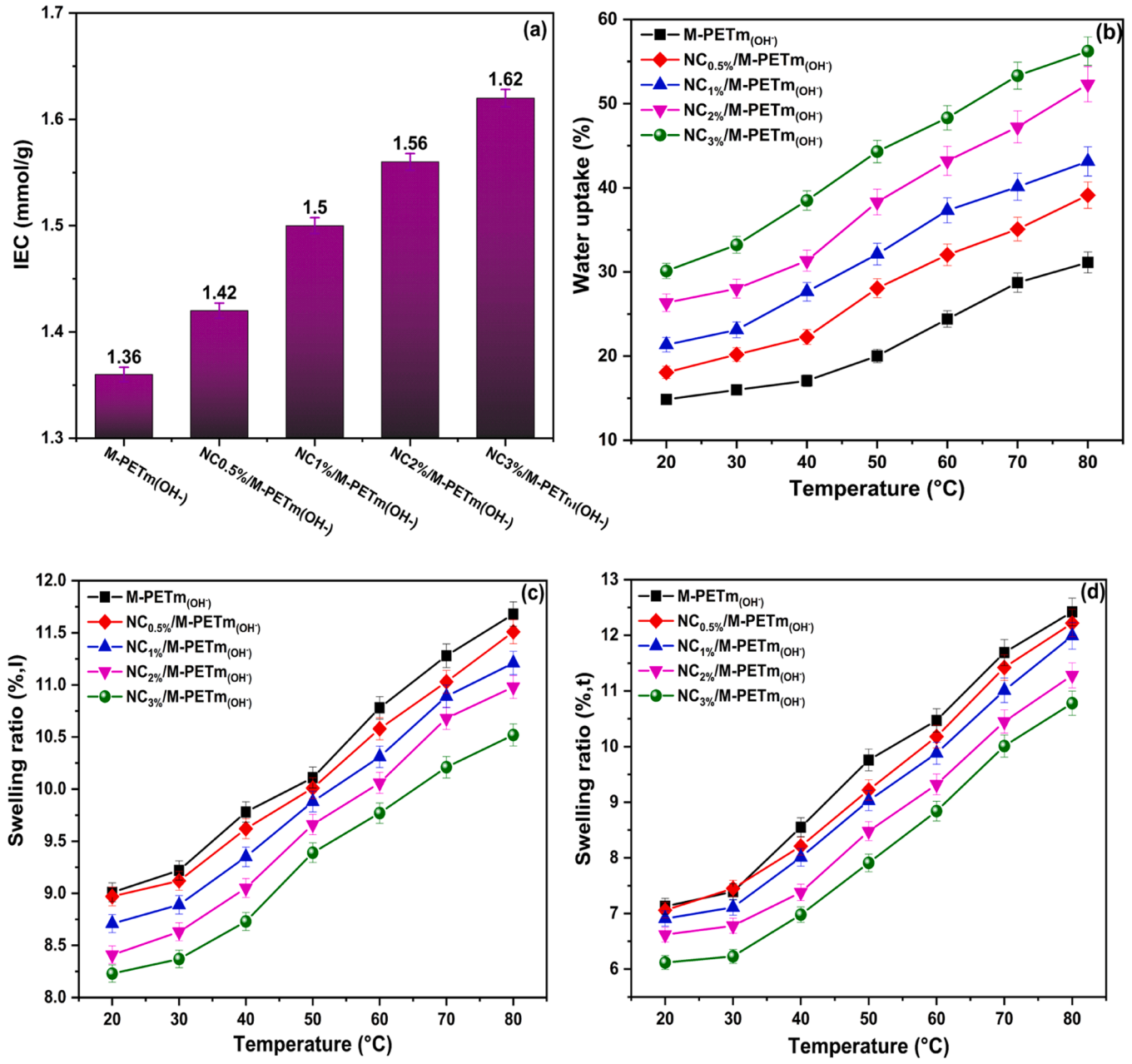

Fig. 8. (a) IEC (b)WU, (c, d) SR (length(l) & thickness(t)) at 20–80 °C in water for M-PETm$_{iOH}$ and NC/M-PETm$_{iOH}$ (0.5,1,2,3 %).

WU and SR values. As temperature increases from 20 to 80 °C, a higher WU for all membranes is observed. This increment is ascribed to the enhanced swelling and the greater polymer chain mobility, which allow for the accommodation of a larger number of water molecules. Moreover, the addition of nanoparticles facilitated water adsorption owing to the water solvation of the additional QA groups [35,58]. The NC$_3$ $_{\%}$/M-PETm$_{iOH}$ experienced the most pronounced increase (from 30.12 % to 56.23 % at 20° and 80 °C), indicating the enhanced WU over M-PETm$_{iOH}$, which shows values of 14.85 % and 31.14 % under the same conditions. Despite the increased water content, all NC$_3$ $_{\%}$/M-PETm$_{iOH}$ displayed lower swelling ratios than the M-PETm$_{iOH}$, showcasing improved dimensional stability with increasing F-TiO$_2$ content. This behavior could be ascribed to the NH$_2$ group's interaction on the NP surface and the polymer matrix through electrostatic forces and hydrogen bonds, limiting chain mobility and membrane swelling [18,23]. At 80 °C, the hydration number λ increased from 12.72 to 19.27 for M-PETm$_{iOH}$ and NC$_3$ $_{\%}$/M-PETm$_{iOH}$ respectively, showcasing a progressive enhancement in water association with increasing nanoparticle content.

3.7. Hydroxide conductivity of membrane

The hydroxide conductivity (σ) of the produced M-PETm$_{iOH}$ and NC/M-PETm$_{iOH}$ (0.5 %, 1 %, 2 %, and 3 %) were measured from 20 to 80 °C. A positive correlation was observed between conductivity and temperature [22,59]. As depicted in Fig. 9a, the composite membrane displayed significantly enhanced ion conductivity compared to the pristine one. Specifically, the NC$_3$ $_{\%}$/M-PETm$_{iOH}$ exhibited the highest ion conductivity, reaching 126 mS/cm, doubling the conductivity of M-PETm$_{iOH}$ 64 mS/cm at 80 °C. This enhancement is attributable to the higher number of QA groups on the NP's surface and to the higher water content, favoring ionic diffusion. However, beyond 3 wt% NPs, there was a decline in σ, which can be attributed to forming a barrier within the ion pathway, impeding effective ion migration [60]. The Ea values (Fig. 9b)

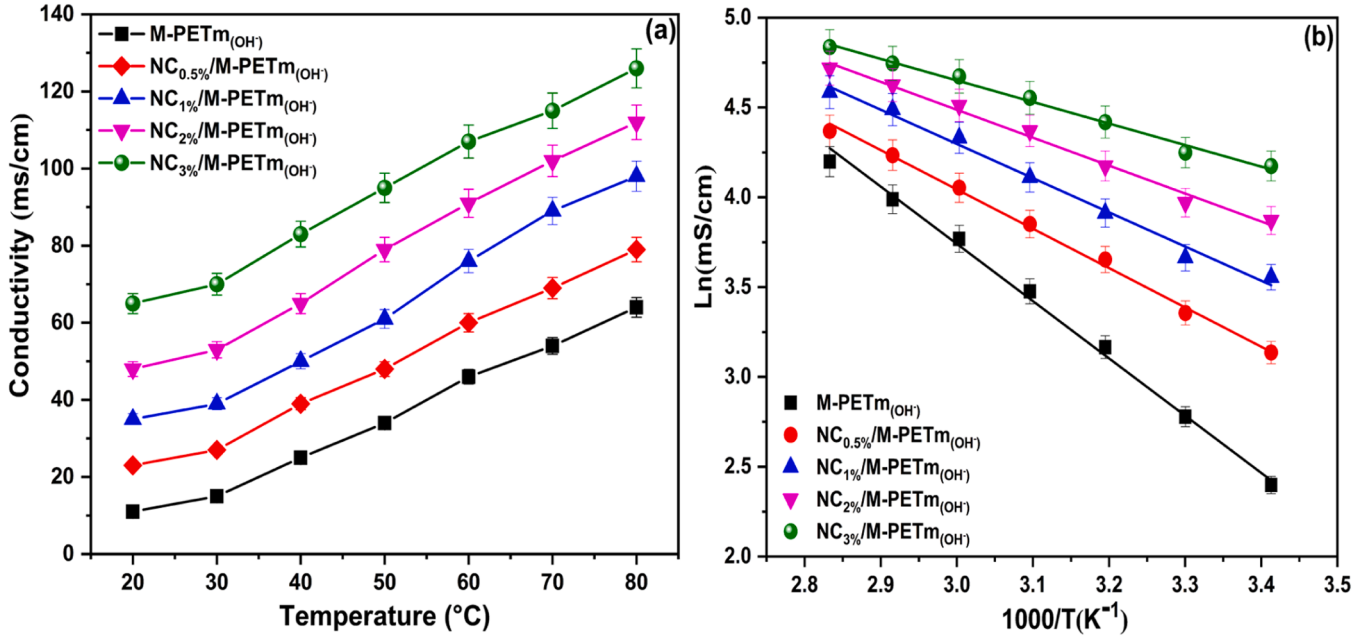

Fig. 9. (a) Ionic conductivity at different temperatures for M-PETm$_{iOH}$ and (0.5,1,2,3 %) NC/M-PETm$_{iOH}$ (b) Arrhenius plot vs temperature.

exhibited a consistent linear trend across all membranes, suggesting that the ion hopping conduction mechanism is dominant. The Ea values (**Table S6**) range between 26.02 and 9.95 kJ mol^{-1} for pristine and NC$_3$ %/M-PETm$_{iOH}$, respectively. Table 1 reports a comparison of recent composite AEMs containing functionalized nanoparticles. The table shows the highest hydroxide conductivities obtained at the maximum testing temperature. Our findings indicate a superiority in IEC and conductivity compared to previous studies.

3.8. Alkaline stability & oxidative stability

Ensuring AEM's long-term stability in alkaline conditions is paramount, given the susceptibility of both functional groups and polymer backbone to OH$^-$ attack, mainly caused by nucleophilic substitution and Hoffman elimination reactions [61,62]. M-PETm$_{iOH}$ and NC$_3$ %/M-PETm$_{iOH}$ stability has been tested by soaking for 20 days the samples in 2 M KOH solution at 80 °C. NC/M-PETm$_{iOH}$ with 3 wt% of F-TiO$_2$ has been chosen as it exhibited the highest conductivity, thus providing a meaningful comparison with the pristine membrane. The results (Fig. 10a) reveal that M-PETm$_{iOH}$ retained 85.8 % of its original conductivity, whereas NC$_3$ %/M-PETm$_{iOH}$ preserved 92.2 % of conductivity. The introduction of F-TiO$_2$ enhanced chemical stability. Such an improvement can be ascribed to the higher water retention of the nanocomposite membrane, which effectively lowers the concentration of cations and mitigates the attack of OH$^-$ ions thanks to the shielding effect of water [63,64]. It is also hypothesized that nanoparticles may act as barriers, hindering the access of OH$^-$ ions to the amine functional groups in the membrane, while providing the grafted 3-silane groups as sacrificial cations to be attacked by the anionic species. These outcomes prove how the incorporation of functionalized fillers assists in an overall improvement of the membrane's physio-chemical properties.

The structure of the polymer backbone directly impacts the membrane's ability to withstand oxidative assaults from hydroxyl and peroxyl radicals [22]. Fig. 10b illustrates the oxidative stability of M-PETm$_{iOH}$ and NC$_3$ %/M-PETm$_{iOH}$ when exposed to Fenton's reagent at 80 °C. Nanocomposite membranes exhibited superior performance compared to pristine ones. Over the testing period, a gradual weight loss was observed. M-PETm$_{iOH}$ experienced slight weight loss after just one day, indicating its susceptibility to radical attacks. In contrast, NC$_3$ %/M-PETm$_{iOH}$ maintained the original weight for three days before exhibiting a marginal loss. After 10 days of testing, it retained 95.5 % weight, while pristine membranes showed only 88.21 % weight retention.

Table 1
Literature overview of IEC and hydroxide conductivity for different nanocomposite AEMs.

Nanocomposite AEMs	IEC (mmol g^{-1})	σ (mS/cm)	Reference
NC$_3$ %/M-PETm$_{iOH}$	1.62	126 (80 °C)	This work
QPAE/GO-(APTS-c-PTMA) 0.7 wt %	1.45	114.2 (90 °C)	[25]
qPSU/NIM-*N*+	1.30	110 (80 °C)	[71]
QPAEK/*f*-TiO$_2$ 5 wt%	1.36	74.6 (90 °C)	[42]
QPAEK-CN-2.0	1.29	21.3 (80 °C)	[68]
MPPO-1.0 wt%sZrO2	1.20	88.7 (80 °C)	[35]

3.9. Thermal stability

The thermal stability of F-TiO$_2$, M-PETm, and NC$_3$ %/M-PETm was determined via TGA. In Fig. 11, the weight loss of F-TiO$_2$ is displayed in blue. A first weight loss of about 4 % (up to 100 °C) is attributable to the evaporation of the absorbed water on the surface of the NP, whereas the additional loss of about 8.4 % spotted between 100 °C and 500 °C is attributed to the combustion of the silane coupling agent [65]. This consistent weight loss constitutes an additional clue for the effective functionalization of the nanoparticles, as pure TiO$_2$ notably exhibits negligible losses in the same range of temperatures [66,67].

For each membrane, distinct three-step decomposition profiles are visible. The initial weight losses of 8.88 % (M-PETm) and 5.44 % (NC$_3$ %/M-PETm), recorded between 50 °C and 90 °C, are caused by the removal of absorbed water and residual solvent. A second weight loss of 25.49 % and 10.42 % for M-PETm and NC$_3$ %/M-PETm, respectively, is observed between 120 °C and 340 °C, and it is associated with the QA group's degradation. The third stage, beyond 400 °C, points out the polymer's backbone degradation. Upon the introduction of F-TiO$_2$, a notable enhancement in thermal stability (up to 330 °C) is observed compared to M-PETm, testifying to the improved resilience of the composite membrane. These findings confirm that composite membranes exhibit thermal properties that are well-suited for electrochemical applications, indicating a promising avenue for their

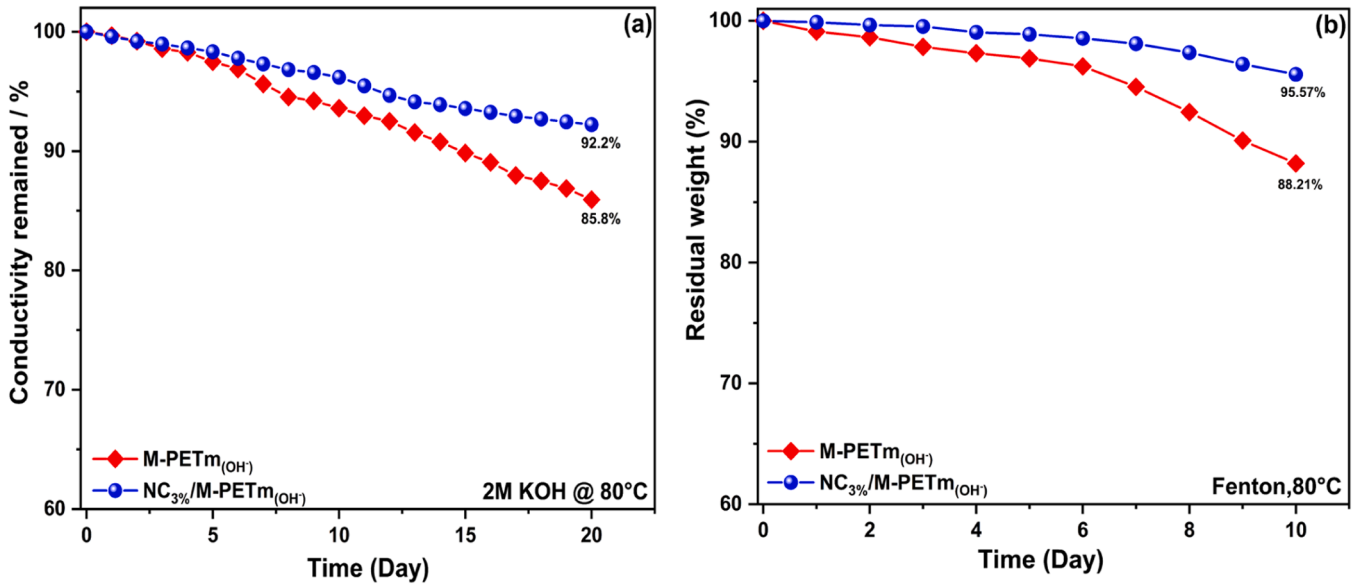

Fig. 10. (a) Alkaline stability of M-PETm$_{iOH}$ and NC$_{3\ \%}$/M-PETm$_{iOH}$ in 2 M KOH at 80 °C, (b) Oxidative stability to the Fenton reagent at 80 °C.

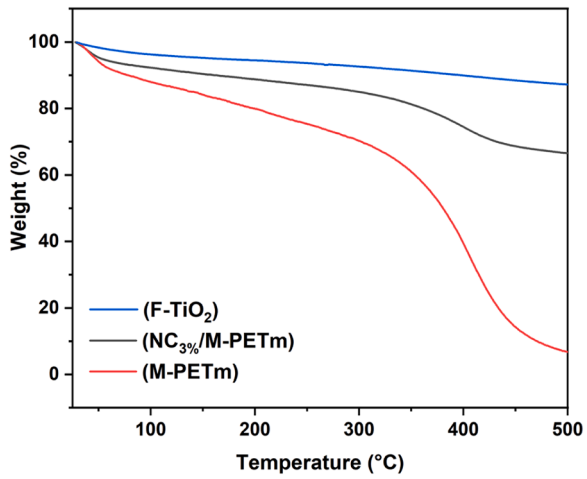

Fig. 11. TGA curves for F-TiO$_2$, NC$_{3\ \%}$/M-PETm, and M-PETm.

utilization in such contexts.

4. Conclusion

This study elucidates the pivotal role of functionalized titanium oxide (F-TiO$_2$) nanoparticles in enhancing the performance of AEMs derived from chemical modification of PET bottles. The structure of the modified PET obtained by aminolysis depolymerization was confirmed by FTIR, extensive NMR experiments, ESI-MS, and HPLC-ESIMS analyses. The successful synthesis of F-TiO$_2$ was confirmed via a thorough characterization, including FTIR, UV, XRD, and TEM analyses. Composite membranes were crafted by incorporating varying concentrations of F-TiO$_2$ (0.5, 1, 2, and 3 wt %) into an M-PETm matrix. Such membranes exhibited an evident enhancement in water retention capability, swelling resistance, and thermal stability compared to pristine ones. Moreover, an overall increase in ionic conductivity was detected upon adding the F-TiO$_2$, due to the enhanced WU and IEC. The composite membrane with 3wt% of nanoparticles emerged as the frontrunner, showcasing the maximum σ of 126 mS/cm at 80 °C. Furthermore, the nanocomposite membranes exhibited good oxidation stability up to 96 % of remaining mass and heightened chemical stability, retaining up to 92 % of conductivity in harsh alkaline conditions after 20 days. The results demonstrate that F-TiO$_2$, which features a tail equipped with amine functional groups, serves a twofold objective: enhancing membrane stability through TiO$_2$ while facilitating the transport of hydroxide ions (OH^-) via the additional functional groups. These encouraging results emphasize the suitability of NC/M-PETm membranes in electrochemical applications, particularly with the merit of utilizing waste PET bottles as raw materials.

Author contributions

The manuscript was a collaborative effort among all authors, with each making significant contributions. Furthermore, all authors have granted their approval for the final version of the manuscript.

Declaration of competing interest

The authors declare that they have no known competing financial interests or personal relationships that could have appeared to influence the work reported in this paper.

Acknowledgments

The authors gratefully acknowledge Programma Operativo Nazionale (PON) 2014–2020 on Innovation and Green, which supports this research activity; the Italian Ministry of Universities and Research (MUR), in the framework of the project DICAM-EXC (Departments of Excellence 2023–2027, grant L232/2016); the European Synchrotron Radiation Facility (ESRF) for provision of synchrotron radiation facilities. We thank the Momentum Transfer team for facilitating the measurements and Jakub Drnec for assistance and support in using beamline ID31. The measurement setup was developed with funding from the European Union's Horizon 2020 research and innovation program under the STREAMLINE project (grant agreement ID 870313).

Supplementary materials

Supplementary material associated with this article can be found, in the online version, at doi:10.1016/j.electacta.2024.145170.

References

[1] C. Santoro, A. Lavacchi, P. Mustarelli, V. Di Noto, L. Elbaz, D.R. Dekel, et al., What is next in anion-exchange membrane water electrolyzers? bottlenecks, benefits, and future, ChemSusChem 15 (2022), https://doi.org/10.1002/cssc.202200027.

[2] J.R. Varcoe, P. Atanassov, D.R. Dekel, A.M. Herring, M.A. Hickner, P.A. Kohl, et al., Anion-exchange membranes in electrochemical energy systems, Energy Environ. Sci. 7 (2014) 3135–3191, https://doi.org/10.1039/c4ee01303d.

[3] S. Pal, R. Mondal, A.K.S. Chandel, U. Chatterjee, Composite anion exchange membranes with antibacterial properties for desalination and fluoride ion removal, ACS EST Water 1 (2021) 2206–2216, https://doi.org/10.1021/acsestwater.1c00147.

[4] M. Mandal, Recent advancement on anion exchange membranes for fuel cell and water electrolysis, ChemElectroChem 8 (2021) 36–45, https://doi.org/10.1002/celc.202001329.

[5] S. Gottesfeld, D.R. Dekel, M. Page, C. Bae, Y. Yan, P. Zelenay, et al., Anion exchange membrane fuel cells: current status and remaining challenges, J. Power Sources 375 (2018) 170–184, https://doi.org/10.1016/j.jpowsour.2017.08.010.

[6] D. Chen, M.A. Hickner, E. Agar, E.C. Kumbur, Optimized anion exchange membranes for vanadium redox flow batteries, ACS Appl. Mater. Interfaces 5 (2013) 7559–7566, https://doi.org/10.1021/am401858r.

[7] W.E. Mustain, M. Chatenet, M. Page, Y.S. Kim, Durability challenges of anion exchange membrane fuel cells, Energy Environ. Sci. 13 (2020) 2805–2838, https://doi.org/10.1039/d0ee01133a.

[8] S. Gottesfeld, D.R. Dekel, M. Page, C. Bae, Y. Yan, P. Zelenay, et al., Anion exchange membrane fuel cells: current status and remaining challenges, J. Power Sources 375 (2018) 170–184, https://doi.org/10.1016/j.jpowsour.2017.08.010.

[9] M.G. Marino, J.P. Melchior, A. Wohlfarth, K.D. Kreuer, Hydroxide, halide and water transport in a model anion exchange membrane, J. Memb. Sci. 464 (2014) 61–71, https://doi.org/10.1016/j.memsci.2014.04.003.

[10] E. Tomasino, B. Mukherjee, V.D. Neelalochana, P. Scardi, N. Ataollahi, Computational modeling of hydrated polyamine-based anion exchange membranes via molecular dynamics simulation, J. Phys. Chem. C 128 (2024) 623–634, https://doi.org/10.1021/acs.jpcc.3c07118.

[11] M. Hren, M. Božič, D. Fakin, K.S. Kleinschek, S. Gorgieva, Alkaline membrane fuel cells: anion exchange membranes and fuels, Sustain Energy Fuels 5 (2021) 604–637, https://doi.org/10.1039/d0se01373k.

[12] D. Henkensmeier, M. Najibah, C. Harms, J. Žitka, J. Hnát, K. Bouzek, Overview: state-of-the art commercial membranes for anion exchange membrane water electrolysis, J. Electrochem. Energy Convers. Storage 18 (2021), https://doi.org/10.1115/1.4047963.

[13] Y. Luo, C. Zhang, B. Zheng, X. Geng, M. Debliquy, Hydrogen sensors based on noble metal doped metal-oxide semiconductor: a review, Int. J. Hydrogen Energy 42 (2017) 20386–20397, https://doi.org/10.1016/j.ijhydene.2017.06.066.

[14] A. Katzfuß, S. Poynton, J. Varcoe, V. Gogel, U. Storr, J. Kerres, Methylated polybenzimidazole and its application as a blend component in covalently cross-linked anion-exchange membranes for DMFC, J. Memb. Sci. 465 (2014) 129–137, https://doi.org/10.1016/j.memsci.2014.04.004.

[15] M. Babaei, M. Jalilian, K. Shahbaz, Chemical recycling of Polyethylene terephthalate: a mini-review, J. Environ. Chem. Eng. 12 (2024) 112507, https://doi.org/10.1016/j.jece.2024.112507.

[16] D.A. Mersha, T.N. Gesese, Z.B. Sendekie, A.T. Admase, A.J. Bezie, Operating conditions, products and sustainable recycling routes of aminolysis of polyethylene terephthalate (PET) – a review, Polym. Bull. (2024), https://doi.org/10.1007/s00289-024-05259-0.

[17] P. Gupta, S. Bhandari, Chemical Depolymerization of PET Bottles via Ammonolysis and Aminolysis, Elsevier Inc., 2019, https://doi.org/10.1016/b978-0-12-811361-5.00006-7.

[18] Y. Zhu, Z. Mao, C. Gao, Aminolysis-based surface modification of polyesters for biomedical applications, RSC Adv. 3 (2013) 2509–2519, https://doi.org/10.1039/c2ra22358a.

[19] N. Rabiei, M. Haghighat Kish, Modification of poly(ethylene terephthalate) fibers, fabrics, and films by amination reactions—a review, Polym. Adv. Technol. 35 (2024) 1–15, https://doi.org/10.1002/pat.6326.

[20] K. Chan, A. Zinchenko, Conversion of waste bottles' PET to a hydrogel adsorbent via PET aminolysis, J. Environ. Chem. Eng. 9 (2021) 106129, https://doi.org/10.1016/j.jece.2021.106129.

[21] A. Mirjalili, B. Dong, P. Pena, C.S. Ozkan, M. Ozkan, Upcycling of polyethylene terephthalate plastic waste to microporous carbon structure for energy storage, Energy Storage 2 (2020) 1–12, https://doi.org/10.1002/est2.201.

[22] V. Donnakatte Neelalochana, E. Tomasino, R. Di Maggio, O. Cotini, P. Scardi, S. Mammi, et al., Anion exchange membranes based on chemical modification of recycled PET bottles, ACS Appl. Polym. Mater. 5 (2023) 7548–7561, https://doi.org/10.1021/acsapm.3c01391.

[23] J.Y. Chu, K.H. Lee, A.R. Kim, D.J. Yoo, Improved electrochemical performance of composite anion exchange membranes for fuel cells through cross linking of the polymer chain with functionalized graphene oxide, J. Memb. Sci. 611 (2020) 118385, https://doi.org/10.1016/j.memsci.2020.118385.

[24] R. Pizzoferrato, E. Ciotta, I.V. Ferrari, R. Narducci, L. Pasquini, A. Varone, et al., Layered double hydroxides containing an ionic liquid: ionic conductivity and use in composite anion exchange membranes, ChemElectroChem 5 (2018) 2781–2788, https://doi.org/10.1002/celc.201800807.

[25] D. Ariono, Khoiruddin, Improving ion-exchange membrane properties by the role of nanoparticles, AIP Conf. Proc. 1788 (2017) 030003, https://doi.org/10.1063/1.4968256.

[26] Ş. Dombaycıoğlu, H. Günsel, A.O. Aydın, Nanofiller-Based novel hybrid composite membranes for high-capacity lithium-sulfur batteries, ChemElectroChem 10 (2023), https://doi.org/10.1002/celc.202300314.

[27] X. Zuo, S. Yu, X. Xu, J. Xu, R. Bao, X. Yan, New PVDF organic-inorganic membranes: the effect of SiO_2 nanoparticles content on the transport performance of anion-exchange membranes, J. Memb. Sci. 340 (2009) 206–213, https://doi.org/10.1016/j.memsci.2009.05.032.

[28] L. Ghassemzadeh, G. Pace, V. Di Noto, K. Müller, Effect of SiO_2 on the dynamics of proton conducting [Nafion/(SiO_2)X] composite membranes: a solid-state 19F NMR study, Phys. Chem. Chem. Phys. 13 (2011) 9327–9334, https://doi.org/10.1039/c0cp02316g.

[29] S.B. Ravikumar, T.A. Mallu, S. Subbareddy, S.A. Shivamurthy, V.D. Neelalochana, K.C. Shantakumar, et al., An enhanced non-enzymatic electrochemical sensor based on the Bi_2S_3-TiO_2 nanocomposite with HNTs for the individual and simultaneous detection of 4-nitrophenol and nitrofurantoin in environmental samples, J. Mater. Chem. B (2024), https://doi.org/10.1039/d3tb03054g.

[30] J. Adebahr, A.S. Best, N. Byrne, P. Jacobsson, D.R. MacFarlane, M. Forsyth, Ion transport in polymer electrolytes containing nanoparticulate TiO_2: the influence of polymer morphology, Phys. Chem. Chem. Phys. 5 (2003) 720–725, https://doi.org/10.1039/b208454f.

[31] P. Salarizadeh, M. Javanbakht, S. Pourmahdian, Enhancing the performance of SPEEK polymer electrolyte membranes using functionalized TiO_2 nanoparticles with proton hopping sites, RSC Adv. 7 (2017) 8303–8313, https://doi.org/10.1039/c6ra25959f.

[32] J. Krzak, A. Szczurek, B. Babiarczuk, J. Gąsiorek, B. Borak, Sol–gel surface functionalization regardless of form and type of substrate. Handb. Nanomater. Manuf. Appl., Elsevier, 2020, pp. 111–147, https://doi.org/10.1016/B978-0-12-821381-0.00005-3.

[33] N. Ataollahi, E. Tomasino, O. Cotini, R. Di Maggio, Enhanced OH− conductivity for fuel cells with anion exchange membranes, based on modified terpolymer polyketone and surface functionalized silica, Energies 15 (2022) 1953, https://doi.org/10.3390/en15051953.

[34] D.N. Varun, J.G. Manjunatha, N. Hareesha, S. Sandeep, P. Mallu, C.S. Karthik, et al., Simple and sensitive electrochemical analysis of riboflavin at functionalized carbon nanofiber modified carbon nanotube sensor, Monatsh. Chem. 152 (2021) 1183–1191, https://doi.org/10.1007/s00706-021-02839-y.

[35] M. Moghadasi, H.R. Mortaheb, Incorporating functionalized silica nanoparticles in polyethersulfone-based anion exchange nanocomposite membranes, J. Appl. Polym. Sci. 134 (2017) 1–13, https://doi.org/10.1002/app.44596.

[36] H. Wu, X. Shen, T. Xu, W. Hou, Z. Jiang, Sulfonated poly(ether ether ketone)/amino-acid functionalized titania hybrid proton conductive membranes, J. Power Sources 213 (2012) 83–92, https://doi.org/10.1016/j.jpowsour.2012.04.003.

[37] K.H. Lee, J.Y. Chu, A.R. Kim, H.G. Kim, D.J. Yoo, Functionalized TiO_2 mediated organic-inorganic composite membranes based on quaternized poly(arylene ether ketone) with enhanced ionic conductivity and alkaline stability for alkaline fuel cells, J. Memb. Sci. 634 (2021) 119435, https://doi.org/10.1016/j.memsci.2021.119435.

[38] N. Ataollahi, E. Cappelletto, K. Vezzù, V. Di Noto, G. Cavinato, E. Callone, et al., Properties of anion exchange membrane based on polyamine: effect of functionalized silica particles prepared by sol–gel method, Solid State Ionics 322 (2018) 85–92, https://doi.org/10.1016/j.ssi.2018.04.022.

[39] C. Simari, A. Caprì, M.H. Ur Rehman, A. Enotiadis, I. Gatto, V. Baglio, et al., Composite anion exchange membranes based on polysulfone and silica nanoscale ionic materials for water electrolyzers, Electrochim. Acta 462 (2023) 142788, https://doi.org/10.1016/j.electacta.2023.142788.

[40] H. Liu, J. Zhou, H. Huang, Amine-functionalized TiO2 nanoparticles for highly selective enrichment of phosphopeptides, Talanta 143 (2015) 431–437, https://doi.org/10.1016/j.talanta.2015.05.019.

[41] M.C. Brochier Salon, M.N. Belgacem, Competition between hydrolysis and condensation reactions of trialkoxysilanes, as a function of the amount of water and the nature of the organic group, Colloids Surf. A Physicochem. Eng. Asp. 366 (2010) 147–154, https://doi.org/10.1016/j.colsurfa.2010.06.002.

[42] J. Pan, J. Han, L. Zhu, M.A. Hickner, Cationic side-chain attachment to poly (phenylene oxide) backbones for chemically stable and conductive anion exchange membranes, Chem. Mater. 29 (2017) 5321–5330, https://doi.org/10.1021/acs.chemmater.7b01494.

[43] Z. Derbali, A. Fahs, J.F. Chailan, I.V. Ferrari, M.L. Di Vona, P. Knauth, Composite anion exchange membranes with functionalized hydrophilic or hydrophobic titanium dioxide, Int. J. Hydrogen Energy 42 (2017) 19178–19189, https://doi.org/10.1016/j.ijhydene.2017.05.208.

[44] J. Zhao, M. Milanova, M.M.C.G. Warmoeskerken, V. Dutschk, Surface modification of TiO2 nanoparticles with silane coupling agents, Colloids Surf. A Physicochem. Eng. Asp. 413 (2012) 273–279, https://doi.org/10.1016/j.colsurfa.2011.11.033.

[45] E. Bakangura, L. Wu, L. Ge, Z. Yang, T. Xu, Mixed matrix proton exchange membranes for fuel cells: state of the art and perspectives, Prog. Polym. Sci. 57 (2016) 103–152, https://doi.org/10.1016/j.progpolymsci.2015.11.004.

[46] A.E. Danks, S.R. Hall, Z. Schnepp, The evolution of "sol-gel" chemistry as a technique for materials synthesis, Mater. Horizons 3 (2016) 91–112, https://doi.org/10.1039/c5mh00260e.

[47] S.M. Ennaceur, J.M. Sanderson, Micellar aggregates formed following the addition of hexafluoroisopropanol to phospholipid membranes, Langmuir 21 (2005) 552–561, https://doi.org/10.1021/la048109y.

[48] S.W. Thomas, G.D. Joly, T.M. Swager, Chemical sensors based on amplifying fluorescent conjugated polymers, Chem. Rev. 107 (2007) 1339–1386, https://doi.org/10.1021/cr0501339.

[49] N. Hareesha, D.M. Soumya, Manjunatha JG Mounesh, R.N. Rohit, P. Manikanta, et al., Honeycomb polypore biomass-derived activated porous carbon nanosheets/graphite/nafion composite: green and sensitive electrocatalyst for nanomolar detection of Hg2+ ions and water-splitting reactions, J. Environ. Chem. Eng. 12 (2024) 113584, https://doi.org/10.1016/j.jece.2024.113584.
[50] A.R.M. Dalod, L. Henriksen, T. Grande, M.A. Einarsrud, Functionalized TiO2 nanoparticles by single-step hydrothermal synthesis: the role of the silane coupling agents, Beilstein J. Nanotechnol. 8 (2017) 304–312, https://doi.org/10.3762/bjnano.8.33.
[51] K.H. Lee, J.Y. Chu, A.R. Kim, H.G. Kim, D.J. Yoo, Functionalized TiO2 mediated organic-inorganic composite membranes based on quaternized poly(arylene ether ketone) with enhanced ionic conductivity and alkaline stability for alkaline fuel cells, J. Memb. Sci. 634 (2021) 119435, https://doi.org/10.1016/j.memsci.2021.119435.
[52] A.A. Coelho, TOPAS and TOPAS-ACADEMIC: an optimization program integrating computer algebra and crystallographic objects written in C++, J. Appl. Crystallogr. 51 (2018) 210–218, https://doi.org/10.1107/S1600576718000183.
[53] P. Scardi, M.A. Malagutti, Thermal diffuse scattering from nanocrystalline systems, Cryst. Growth Des. (2023), https://doi.org/10.1021/acs.cgd.3c01507.
[54] P. Scardi, C.L. Azanza Ricardo, C. Perez-Demydenko, A.A Coelho, Whole powder pattern modelling macros for TOPAS, J. Appl. Crystallogr. 51 (2018) 1752–1765, https://doi.org/10.1107/S160057671801289X.
[55] E. Bakangura, L. Wu, L. Ge, Z. Yang, T. Xu, Mixed matrix proton exchange membranes for fuel cells: state of the art and perspectives, Prog. Polym. Sci. 57 (2016) 103–152, https://doi.org/10.1016/j.progpolymsci.2015.11.004.
[56] D.L. Zapata-Tello, V. Escobar-Barrios, J.A. Gonzalez-Calderon, E. Pérez, Chemical modification of titanium dioxide nanoparticles with dicarboxylic acids to mediate the UV degradation in polyethylene films, Polym. Bull. 77 (2020) 6409–6431, https://doi.org/10.1007/s00289-019-03066-6.
[57] K.H. Lee, J.Y. Chu, A.R. Kim, H.G. Kim, D.J. Yoo, Functionalized TiO2 mediated organic-inorganic composite membranes based on quaternized poly(arylene ether ketone) with enhanced ionic conductivity and alkaline stability for alkaline fuel cells, J. Memb. Sci. 634 (2021) 119435, https://doi.org/10.1016/j.memsci.2021.119435.
[58] M. Garmsiri, H.R. Mortaheb, M. Moghadasi, Effects of functionalized silica nanoparticles on characteristics of nanocomposites PES cation exchange membranes, J. Wuhan Univ. Technol. Mater. Sci. Ed. 32 (2017) 1239–1249, https://doi.org/10.1007/s11595-017-1737-0.
[59] T.Y. Son, T.H. Ko, V. Vijayakumar, K. Kim, Nam SY, Anion exchange composite membranes composed of poly(phenylene oxide) containing quaternary ammonium and polyethylene support for alkaline anion exchange membrane fuel cell applications, Solid State Ionics 344 (2020) 115153, https://doi.org/10.1016/j.ssi.2019.115153.
[60] Q. Che, L. Zhou, J. Wang, Fabrication and characterization of phosphoric acid doped imidazolium ionic liquid polymer composite membranes, J. Mol. Liq. 206 (2015) 10–18, https://doi.org/10.1016/j.molliq.2015.01.054.
[61] R. Espiritu, J.L. Tan, L.H. Lim, S. Arco, Density functional theory study on the degradation of fuel cell anion exchange membranes via removal of vinylbenzyl quaternary ammonium head group, J. Phys. Org. Chem. 33 (2020) 1–10, https://doi.org/10.1002/poc.4049.
[62] X. Chu, J. Liu, S. Miao, L. Liu, Y. Huang, E. Tang, et al., Crucial role of side-chain functionality in anion exchange membranes: properties and alkaline fuel cell performance, J. Memb. Sci. 625 (2021) 119172, https://doi.org/10.1016/j.memsci.2021.119172.
[63] X. Zhang, Z. Yu, J. Tang, J. Huang, X. Tang, B. Lin, et al., Mxenes as inorganic fillers for the construction of poly(aryl piperidinium) anion exchange membranes with microphase separation structures to enhance ionic conductivity, Fuel 365 (2024) 131177, https://doi.org/10.1016/j.fuel.2024.131177.
[64] D.R. Dekel, M. Amar, S. Willdorf, M. Kosa, S. Dhara, C.E. Diesendruck, Effect of water on the stability of quaternary ammonium groups for anion exchange membrane fuel cell applications, Chem. Mater. 29 (2017) 4425–4431, https://doi.org/10.1021/acs.chemmater.7b00958.
[65] X.W. Li, R.G. Song, Y. Jiang, C. Wang, D. Jiang, Surface modification of TiO_2 nanoparticles and its effect on the properties of fluoropolymer/TiO2 nanocomposite coatings, Appl. Surf. Sci. 276 (2013) 761–768, https://doi.org/10.1016/j.apsusc.2013.03.167.
[66] M. Asif, M. Zafar, P. Akhter, M. Hussain, W.Y. Kim, A. Umer, et al., Effect of urea addition on anatase phase enrichment and nitrogen doping of tio2 for photocatalytic abatement of methylene blue, Appl. Sci. 11 (2021) 1–15, https://doi.org/10.3390/app11178264.
[67] Y. Wang, J. Yu, W. Peng, J. Tian, C. Yang, Novel multilayer TiO_2 heterojunction decorated by low g-C3N4 content and its enhanced photocatalytic activity under UV, visible and solar light irradiation, Sci. Rep. 9 (2019) 1–15, https://doi.org/10.1038/s41598-019-42438-w.